ELKOMIKA: Jurnal Teknik Energi Elektrik, Teknik Telekomunikasi, & Teknik Elektronika

ISSN(p): 2338-8323 | ISSN(e): 2459-9638 | Vol. 11 | No. 2 | Halaman 479 - 493
DOI : http://dx.doi.org/10.26760/elkomika.v11i2.479 April 2023

Active Control based on Adaptive Filters for Elastic Supported Cylinders

SUBEKTI SUBEKTI[1], NANA SUBARNA[2], SHANTI KUMBARASARI[3], AGUNG WAHYUDI BIANTORO[4]

[1,4]Mechanical Engineering, Universitas Mercu Buana, Jakarta, Indonesia
[2]Electrical Engineering, Institut Teknologi Nasional, Bandung, Indonesia
[3]Mechanical Engineering, Politeknik Industri ATMI, Cikarang, Indonesia
Email : subekti@mercubuana.ac.id

Received 15 Februari 2023 **|** *Revised* 3 Maret 2023 **|** *Accepted* 28 Maret 2023

ABSTRAK

Dalam makalah ini, kami menyajikan strategi kontrol feedforward baru disajikan untuk kontrol getaran induksi aliran dari silinder tabung yang ditopang balok kantilever elastis yang dipasang melintang. Strategi kontrol bertujuan untuk membatasi gerakan dari silinder tabung yang ditopang balok kantilever elastik, untuk mencegah getaran optimal yang akan menghasilkan nonlinear sistem. Sistem control feedforward menggunakan gabungan antara multiresolution wavelet dengan Filtered-x least mean square (FxLMS) control algorithm. Untuk memverifikasi kelayakan algoritme kontrol yang diusulkan, upaya numerik dengan menggunakan persamaan Van der Pol dan hasil penerapan dalam eksperimental dilakukan untuk memperlihatkan respon getaran yang terjadi terhadap waktu. Diperoleh bahwa keefektifan algoritme wavelet-FxLMS sebagai strategi kontrol getaran aktif nonlinear telah berhasil didemonstrasikan baik secara eksperimental maupun teoritis di bawah osilator bangun Van der Pol.

***Kata kunci**: kontrol adaptif, teori kontrol, sistem kontrol, kontrol getaran, sistem kontrol non-linier.*

ABSTRACT

In this paper, we present a novel feedforward control strategy presented for the control of flow-induced vibration of a tube cylinder supported by a transversely mounted elastic cantilever beam. The control strategy aims to limit the movement of the tube cylinder which is supported by elastic cantilever beams, to prevent optimal vibration which will result in a nonlinear system. The feedforward control system uses a combination of multiresolution wavelets and the Filtered-x least mean square (FxLMS) control algorithm. To verify the control feasibility of the proposed algorithm, a numerical effort using Van der Pol equation and the results of implementing it in the experiment was carried out to reveal the response vibrations that occur over time. It was found that the effectiveness of the wavelet-FxLMS algorithm as a nonlinear active vibration control strategy has been successfully demonstrated both experimentally and theoretically under a Van der Pol wake oscillator.

***Keywords**: adaptive control, control theory, control systems, vibration control, non-linear control systems.*

1. INTRODUCTION

The phenomenon of flow vibration caused by vortices formed behind elastically supported cylinders in cross flow has been a challenging problem for many years. Formation Isolation Valve experiments in line on a rotating cylinder with space scale parameters 5 < U6 < 32 and 0 < a < 3.5 include vibration response, moving fluid forces and spatial structures in the fluid system **(Zhao, 2018).**

When the vortex discharge frequency is close to the system's natural frequency, a large amplitude locking and vibration phenomenon will occur. When the reference frequency is declared to be optimal based on a band active noise control system at a minimum scale then most of the results are biased when compared to the original resonant frequency. This shows the non-linear mechanism of the control system **(An, 2022).**

If the velocity of the vibration of the cubic spring and the linear spring decreases and shows the same nominal value, the modulation value of the vibration amplitude gradually decreases but the Reynolds number increases **(Wang, 2019).**

Vortex Induced Vibration suppression and friction reduction at high Re motion flow to absorb non-linear energy. This results in an increase in the power performance of Vortex-Induced Vibration induced in electric current generators **(Blanchard, 2019).**

When the Reynolds number ranges from 16000 to 24500 with a large-scale mass ratio of 248 and a small damping ratio of 0.00257. The speed of the Vortex Induced Vibration will decrease with the initial value of 4.5 to 6.8. This is due to increased three-dimensional interference in the helical cable. Aerodynamic damping in negative oscillating bare cylinders, positive wired cylinders with A/D amplitude vibrations of 1/4 0.1 at the resonant speed of bare cylinders **(Ishihara, 2019).**

Attenuation measurement patterns, virtual sensing techniques and determining the location of sound sources require a feedback system that can reduce interference **(Bean, 2018).** Feedforward and feedback settings by mounting sensors at positions at the beginning and at the end of the actuator results in unstable disturbance at positions at the lower threshold. This is due to the time delay at 5% velocity in convection free flow **(Nibourel, 2022).** So, to overcome the vibration resonance caused, a hybrid H2/generalized H2 control strategy is needed by using Linear Matrix Inequation optimization technology to suppress the horizontal vibration of high-speed elevators **(Cao, 2020).**

The research method of the Adaptive Mode Neuro Fuzzy Inference System (ANFIS) shows the recording of input-output data on a vibrating cylinder system using an accelerometer at a certain time scale resulting in an average squared error system of 3,411 x 10^{-10} **(Shaharuddin, 2013).** After recording, the use of a bilinear functional link neural network (BFLNN) filter for non-linear control is used as feedback on the reference simulation signal and different acoustic paths **(Luo, 2018).**

The use of non-linear active noise control system (NANC) has drawbacks in the computational loading of secondary non-linear paths (NSP) and the convergence system is not optimal **(Cong, 2018).** In an effort to increase vibration reduction, an alternative is made for active noise control (ANC) originating from vibrations to effectively reduce noise levels in electroacoustic or electromechanical systems **(Lu, 2021).**

In this paper, we present the feed-forward active control of the flow-induced vibration of a circular cylinder supported by an elastic cantilever beam. We discuss the simulation of the wake oscillator

represented by the Van der Pol equation **(Kobayashi, 2006)** and an experimental study of the active vibration control using the Filtered Reference Least Mean Square (FxLMS) algorithm based on an adaptive filter.

The use of the FxLMS adaptive filter model can increase, eliminate and neutralize disturbances to the amplitude. Fast Fourier Transform (FFT) analysis can be used to modify the increase or decrease the frequency **(Kant, 2022).** Control logic modeling with Single Input-Output System and Surface Related Multiple Elimination configurations results in the ability of noise reduction structure schemes on all lines of the targeted space **(Botti, 2021).** Many experimental studies (using wavelet filters and FxLMS) have been carried out to explore and understand the characteristics of different types of signals.

An active vibration control n of a rectangular plate representing a flexible wall by means of a control actuator based on FxLMS **(Carra, 2008).** This FxLMS algorithm shows a certain effectiveness of the theoretically optimally placed actuator in the emerging correspondent modal form. The FxLMS system works very well to control systems which include phase delays, multiple sensor inputs, high and nonlinear noise levels in feed-forward systems at turbulent boundary layers **(Morra, 2018).**

A control based on a multi-input-multi-output (MIMO) adaptive algorithm with an x-least-mean-square (fxLMS) filter can display free turbulent flow disturbances with different amplitudes and scales on plasma actuators and shear stress sensors **(Wu, 2006).** An adaptive controller using normalized FxLMS was adopted to cancel the force transmitted through the active engine mount **(Niu, 2019).** Control FxLMS by performing online modeling of adaptively adjusted secondary pathways and step sizes **(Lee, 2000).**

Online modeling of secondary pathways, variable step sizes determined with the FxLMS controller showed improved adaptive control performance over definite time variations **(Fallah, 2019).** Analysis of several properties of observer-based control robustness and adaptive FxLMS for active control of engine-induced vibration in automotive vehicles **(Liang, 2022).** In addition, FxNLMS controller feedback can dampen drill rod vibrations of 70 dB for a depth of 0.2 m on 6063-T6 Aluminum alloy material **(Wenchao, 2019).**

The use of a noise control system The complex recursive x-filtered algorithm (FxRLS) in aircraft and vehicle cabins has certain limitations so that it is necessary to increase robustness and denoising to achieve stability in convergent conditions **(Sun, 2022).**

Wavelet transform has been promoted as a multi-resolution signal processing tool elegant **(Kowalczyk, 2005).** The formation of a non-linear two-dimensional transformation using two sub bands. The structure of two sub bands that are compact, complex values approach the Wringer gradient and uses a Fourier-Argand filter with a steerable filter so that it is able to estimate the amplitude, direction of features with high noise conditions **(Akansu, 2001).**

Morlet wavelet filters are used to detect weak and impulse-like mechanical defects signals **(Qiu, 2006).** Bistable flow characteristics they concluded that spectral analysis using Fourier transform is not appropriate for identifying phenomena and wavelet transform is a very appropriate tool for problem analysis **(Olinto, 2006).** Gloria Adewumi1 and Professor Freddie Inambao **(Adewumi, 2017)** conducted a study on blade noise using an ANC feedback system based on the FxLMS algorithm with MATLAB simulation. Mallat **(Malate, 1989)** investigated the characteristics of bi-stable flow, concluding that although spectral analysis using Fourier transforms is not suitable for identifying phenomena, wavelet transforms are a very appropriate tool for problem analysis. Piotr Krauze and Jerzy Kasprzyk **(El-Shahed, 2022)** conducted research on the rear MR damper

controlled by FxLMS (Filtered-x LMS) by utilizing information about the movement of the vehicle axle, while the purpose of this algorithm is to minimize vehicle body pitch. The DWT-FFT-FXLMS algorithm can effectively remove stationary and non-stationary noise, while the FXLMS frequency domain algorithm (FD-FXLMS) cannot approach this point **(Krause, 2016).**

Based on the multi-resolution stationary hybrid wavelet matrix decomposition technique, it can hide videos with high capacity and imperceptibility **(Qiu, 2016).** The wavelet-based filtered-x LMS is then applied to a nonlinear PMSM system which is subject to a desired angular velocity which is constant and varies harmoniously in time **(Tong, 2014).** the feedback section uses a frequency domain wavelet packet algorithm based on FXLMS multi-resolution analysis (WPFXLMS) to control for uncorrelated disturbances encountered during operation of the ANC system **(Padhi, 2018).** The intrinsic similarity between wavelet filters and noise/vibration signals implies that a better approximation of these signals can be achieved using wavelet filters **(Akraminia, 2017).** modifications were made to the existing FxLMS algorithm which provides a new structure to improve tracking performance and convergence rates. The secondary signal y(n) is dynamically thresholded with a wavelet transform to improve tracking **(Babu, 2010).** Many studies on control systems have been carried out at Mercubuana University, such as making an automatic smoke and gas leak detection system using the Arduino Uno microcontroller. For this reason, it is necessary to create a system that supports monitoring mechanisms in real time and can provide warnings and notifications based on sound media (alarms) and LED lights **(Agung, 2020)**, MACH3 Control Based CNC Lathe Machine Design **(Muslim, 2022)**, The dynamic system modeling in an elastically supported rigid cylinder for electrodynamic vibration energy harvesting **(Subekti1, 2022).** The robotic arm system used was five degree of freedom, which used 5 servo motors in the design **(Subekti2, 2019).**

In this paper, we present the theoretical basis of the multiresolution and the FxLMS algorithm in Section 2 and also describes an elastically supported rigid cylindrical model. Results and discussion, and summaries are presented in Sections 3 and 4, respectively.

2. METHODOLOGY

The FxLMS algorithm is a well-known algorithm for feed-forward active control, which involves canceling noise from the system response to the reference input. The block diagram of an active broadband feed-forward control using the FxLMS algorithm is illustrated in Fig.1, as proposed by (16). Here, $\hat{S}(z)$ is the estimation of the transfer function of the secondary part. The primary disturbance d (n) comes from the convolution of the reference signal x(n) with the response function of the primary pathway P (z). The W(z) adaptive filter must simultaneously model the W(z) primary line and the inverse of the S(z) secondary line.

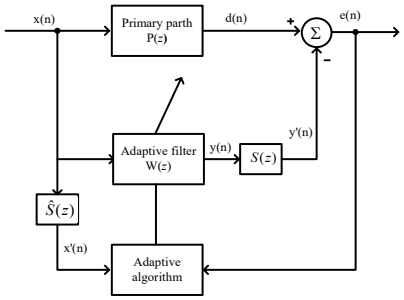

Figure 1. Block diagram of the implementation of the FxLMS algorithm

On figure 1, $S(z)$, which is a secondary path between $e(n)$ and $y(n)$, is modeled offline and maintained during the online operation of the active vibration control. The output of the adaptive filter can be represented as

$$y(n) = w^T(n)\, x\,(n) \tag{1}$$

where $w(n) = [w_0(n) \quad w_1(n) \ \cdots \ w_{L-1}(n)]^T$ is the coefficient vector of the adaptive filter $W(z)$ and the reference signal vector $x(n) = [x(n) \quad x(n-1) \ \cdots \ x(n-L+1)]^T$L × 1 is . The signal $y(n)$ is filtered through the secondary path $S(z)$, and subtracted from the primary fault $d(n)$ to produce the residual error $e(n)$. The equation for the simulation is given as

$$\begin{aligned} d(n) &= P(z) * x(n) \\ y'(n) &= S(z) * y(n) \\ e(n) &= d(n) - y'(n) \end{aligned} \tag{2}$$

where * denotes the convolution operator. All these operations are performed by the system internally. For the adaptive filter, the updated weight vector equation is

$$w(n+1) = w(n) + \mu\ e(n)\ x'(n), \tag{3}$$

where μ is the convergence coefficient, and the filtered reference signal vector is $x'(n) = [x'(n)\ x'(n-1)\ \cdots\ x'(n-L+1)]^T$, which is obtained by filtering the reference signal $x(n)$ with $\hat{S}(z)$,

$$x'(n) = \hat{S}(z) * x(n), \tag{4}$$

Multi-resolution analysis based on wavelet transform allows the decomposition of the signal into various resolution levels. Multi-resolution analysis involves approximating the function in the closed subspace order $\{V_m | m \in Z\}$of $\mathrm{L2\,(R)}$. Next, let the direct number of infinite possible spaces W_m range $\mathrm{L^2\,(R)}$ as

$$\mathrm{L^2\,(R)} = \oplus\, W_m \oplus W_{m-1} \cdot \oplus\, W_0 \oplus W_{-m+1} \oplus W_{-m+2} \tag{5}$$

We start with the scaling function $f(t)$, so translated as $\{f(tn)\}$ spanning V_0. Then V_{-1} is stretched by $f(2tn)$, as an increasing function at V_0.

Thus, *V1 is generated* by the integer translation of the two functions, and $f(t)$ can be expressed as a linear combination of the even and odd translations of $f(2t)$, or

$$\varphi(t) = \sqrt{2}\sum_n h_0(n)\ \ \varphi(2\mathrm{t} - n)\ nR \in \tag{6}$$

The set coefficient $\{h_0(n)\}$ is *the basic coefficient between scales*. Similarly, the wavelet function can be expressed as a linear combination of the translations $f(2\,t)$ as

$$\psi(t) = \sqrt{2}\sum_n h_1(n)\ \ \varphi(2\mathrm{t} - n)\ nR \in \tag{7}$$

Equation (7) is true for some set of wavelet generation coefficients $h_1(n)$, because the wavelet is in the space spanned by a narrower scaling function, $W_0 V_1$ and is called the fundamental wavelet equation. *h1* is the high-pass coefficient that produces the wavelet function, and *h0* is low pass filter that defines the scaling function. Equation (7) generates wavelets directly from the scaling function. Next , we examine the relationship between *h1* and h_0. By taking the Fourier transform of Eq. (7), the high-pass and low-pass filters are therefore related by:

$$h_1(n) = (-1)^n h_0(1-n) \tag{8}$$

Sometimes, we use (1) n 1 in Eq. (8), which inverts the wavelet.

In this paper, where we consider a multi-resolution algorithm, when using the Fourier transform, Eq. (8) can also be changed to

$$\psi(\omega) = \frac{1}{\sqrt{2}} H_1\left(\frac{\omega}{2}\right) \varphi\left(\frac{\omega}{2}\right) \tag{9}$$

Next, we modify the implementation block diagram of the FxLMS algorithm in Figure 1. By examining Eq. (2), the signal $y(n)$ is the output of the multi-resolution filter $y(n) = X(n)* W(n)$, and $y'(n)$ is the signal generated at the fault point of our sensor.

The objective function is

$$J(w) = E\{e^2(n)\} \tag{10}$$

Replacing Eq. (2) into Eq. (10) we get

$$J(w) = E\{[d(n) - y'(n)]^2\} \tag{11}$$

Equation (11) is minimized by updating the weight vector in the negative direction of the half gradient vector given by

$$\frac{1}{2}\frac{\partial J(n)}{\partial w(n)} = -e(n)\frac{\partial y\ (n)}{\partial w(n)} \tag{12}$$

The weight vector $w(n)$ updated in the negative direction of the half gradient vector is

$$w(n+1) = w(n) - \mu\frac{1}{2}\frac{\partial J(n)}{\partial w(n)} \tag{13}$$

Replacing Eq. (12) to Eq. (13) we get

$$w(n+1) = w(n) + \mu e(n)\frac{\partial y'(n)}{\partial n} \tag{14}$$

where m is the convergence coefficient, which must take a small number to ensure the stability of the adaptive algorithm

$$y(n-r) = X(n-r)w(n-r) \tag{15}$$

Assuming $w(n) = w(n-r)$, Eq. (15) can be modified to

$$y(n-r) = X(n-r)w(n) \tag{16}$$

$$\frac{\partial y(n-r)}{\partial w(n)} = X(n-r) \tag{17}$$

We define a derived nonlinear system

$$g(r,n) = \frac{\partial y'(n)}{\partial y(n-r)} \tag{18}$$

Replacing Eq. (18) into Eq. (15), then substitute the result into Eq. (14), we can get the latest function of W(n)

$$w(n+1) = w(n) + \mu e(n) \sum_{r=0}^{M-1} g(r,n) \frac{\partial y(n-r)}{\partial w(n)} \tag{19}$$

Components $\sum_{r=0}^{M-1} g(r,n) \frac{\partial y(n-r)}{\partial w(n)}$ are filtered versions of $\frac{\partial y(n-r)}{\partial w(n)}$, or $X(n-r)$. The coefficient of this filter can be obtained from the input and output of the multi-resolution analysis filter $\hat{S}(z)$; we rewrite Eq. (4) as

$$x'(n) = \hat{S}(z) * X(n) \tag{20}$$

Substitution Eq. (17) into Eq. (3) result

$$w(n+1) = w(n) + \mu\ e(n)\ x'(n) \tag{21}$$

From Eq. (21), (20) and (18), we can now use this algorithm for an active nonlinear vibration control system in the secondary, which is illustrated in Figure 2.

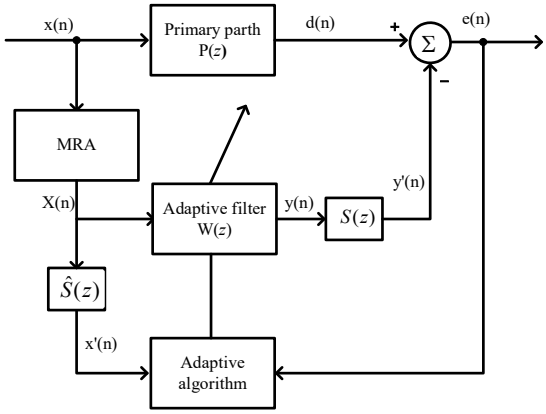

Figure 2. Nonlinear Multi-resolution filter-reference LMS Algorithm

A rigid circular cylinder is supported at two points by an elastic cantilever beam as shown in Fig. 3. Beams are placed outside the wind tunnel test section to avoid disruption to flow.

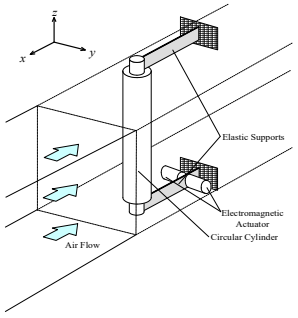

(a) Experimental Setting

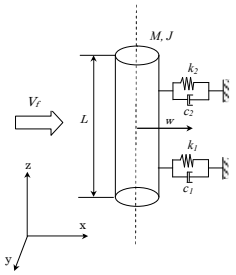

(b) Mathematical Model

Figure 3. Elastically supported rigid cylinder model

The test cylinder has a cross section outside diameter D = 0.045 m, length L = 0.32 m and mass M = 0.06642 kg. Given the transverse oscillation of the cylinder, the equation of motion for the cylinder is derived as:

$$M\ \ddot{y}(t) + C_y\dot{y}(t) + K_y y(t) = u(t) + w(t), \tag{22}$$

where $u(t)$ is the control input, $w(t)$ is the fluctuating lift, M is the mass of the cylinder, C_y is the damping coefficient, and K_y is the stiffness of the beam spring. We assume that the wake oscillator model is expressed as

$$\ddot{v}_f - \varepsilon\omega_f\left(1 - K\dot{v}_f^2\right)\dot{v}_f + \omega_f^2 v_f = \varepsilon_1\ddot{y} + \varepsilon_2\dot{y}, \tag{23}$$

where *vf is the wake-up oscillator* displacement and *wf is the wake*-up frequency. e_1 and e_2 are proportionality coefficients, e are Van der Pol parameters, and K are nonlinear damping coefficients. Distinguishing equation (23) and introduces the dimensionless time $\tau = \omega_f t$and a new variable $z = \sqrt{3\mathrm{K}}\dot{v}_f$, Eq. (23) becomes

$$\ddot{z} + \varepsilon(z^2 - 1)\dot{z} + z = \alpha\ \ddot{y} + \beta\ \ddot{y}, \tag{24}$$

where

$$\alpha = \varepsilon_1\omega_f\sqrt{3\mathrm{K}}\ \text{and}\ \beta = \varepsilon_2\sqrt{3\mathrm{K}}, \tag{25}$$

The fluctuation of the lift force is considered to be proportional to the relative velocity and acceleration as follows:

$$w = m_f\left(\ddot{v}_f - \ddot{y}\right) + c_f\left(\dot{v}_f - \dot{y}\right), \tag{26}$$

where *mf* and *cf* are the additional mass and damping, respectively. Changing the variable using τ and *z*, the equation of motion of the cylinder (26) is rewritten as

$$\ddot{y} + \gamma\ \dot{y} + \kappa\ y = \delta\ \dot{z} + \sigma\ z, \tag{27}$$

Equations (24) and (27) can be rewritten as matrices of

$$\begin{Bmatrix}\dot{x}_1\\ \dot{x}_2\\ \dot{x}_3\\ \dot{u}_1\\ \dot{u}_2\end{Bmatrix} = \begin{Bmatrix}0 & 1 & 0 & 0 & 0\\ \kappa & -\gamma & 0 & \sigma & \delta\\ 0 & \frac{\kappa}{(\delta\alpha-1)} & \frac{(\gamma-\delta\beta)}{(\delta\alpha-1)} & \frac{\delta}{(\delta\alpha-1)} & -\frac{\left(\sigma\cdot u_2-\delta\varepsilon\left(u_1{}^2-1\right)\right)}{(\delta\alpha-1)}\\ 0 & 0 & 0 & 0 & 1\\ 0 & \left(\frac{\kappa}{\delta(\delta\alpha-1)}+\frac{\kappa}{\delta}\right) & \left(\frac{(\gamma-\delta\beta)}{\delta(\delta\alpha-1)}+\frac{\gamma}{\delta}\right) & \frac{\delta}{\delta(\delta\alpha-1)} & \left(\frac{\left(\sigma\cdot u_2-\delta\varepsilon\left(u_1{}^2-1\right)\right)}{\delta(\delta\alpha-1)}+\frac{\sigma}{\delta}\right)\end{Bmatrix}\begin{Bmatrix}x_1\\ x_2\\ x_3\\ u_1\\ u_2\end{Bmatrix} \tag{28}$$

Where $x_1 = y,\ x_2 = \dot{y},\ x_3 = \ddot{y},\ u_1 = z,\ u_2 = \dot{z}.$
The time history response of the Van der Pol oscillator model is simulated by integrating Eq. (28) numerically. The details of the coefficients in the above equation are omitted due to space limitations.

3. RESULTS AND DISCUSSION

The experimental setup is shown in Fig. 3(a). The cylinders and supporting beams are made of polycarbonate and steel, respectively. The parameters used in this study were κ= 0.008, γ = 296, δ = 1.7, δ= *0.01* , α = *0.96* , σ = *5.43 x10* $^{-3}$, ε = 0.92 x 10 $^{-5}$, and the initial conditions were $x_1 = 0$, $x_2 = 0.001$, $x_3 = 0$ and $u_1 = 0$, $u_2 = 0.001$.

The experimental results using the wavelet-FxLMS algorithm with a comparative case study of the FxLMS algorithm are detailed in this section. The input reference is taken from wake oscillations, measured using a displacement sensor. An active nonlinear vibration control system, namely an electromagnet (EMA), is used as the control actuator. They are set 15 mm apart from the fixed end of the plate and the space between the magnet and the beam is 1 mm. The attraction of the electromagnet depends on its distance from the block. We estimate the attractive force from the experimental data, $F = 1.360\ V^2$. Due to the limitations of the amplifier, the maximum voltage of the magnet is 12 V.

Figure 4 shows (a) the experimental signal and (b) the spectrum of the output power at a flow rate of 6.4 m/s. The blue line shows the output power spectrum when no compensation is used. The red and black lines indicate the output power spectrum, respectively, when the FxLMS and wavelet-FxLMS adaptive filter algorithms are used. Note that for the FxLMS case, the output is greatly reduced by about 30 dB at 2 Hz. However, at 3.4 Hz, the output increases by 38 dB. It is different when we use wavelet-FxLMS, wavelet-FxLMS can reduce the frequency at all 30dB. From Figure 4, we can conclude that the nonlinear system can be reduced more effectively by the wavelet-FxLMS approximation.

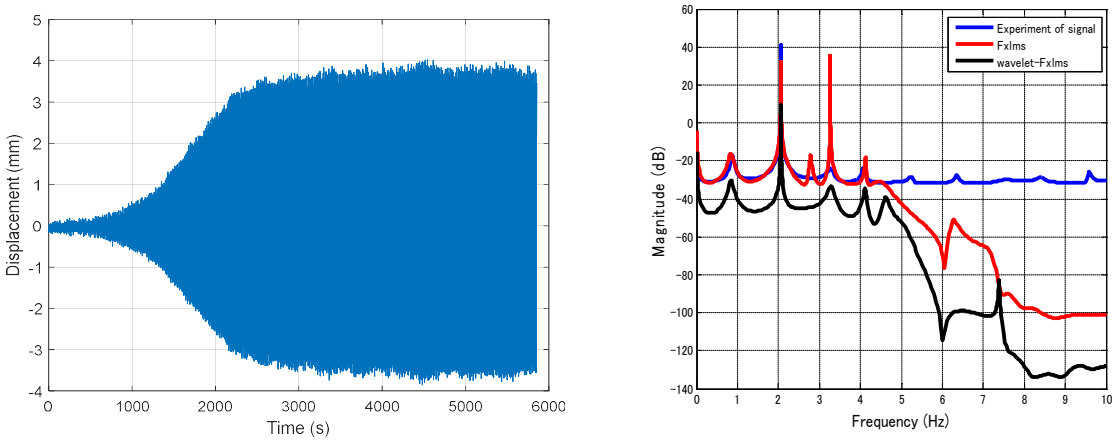

(a) Signal test **(b) Power spectrum**

Figure 4. Experimental vortex induction cylinder at a flow velocity of 6.4 m/s

Figure 5 shows that the results of signal measurements (Fig. 5(a)) and the results of Fast Fourier Transform (FFT) (Fig. 5(b)). The low-pass filter (Fig. 5(a) at the bottom) signal approaches the signal after noise reduction at high frequencies. The high-pass filtered (Fig. 5(a) the center section) signal represents the noise removed, and is the difference between the measured signal and the low-pass filtered signal. he Fast Fourier transform of the measured signal is presented in Fig. 5(b), as well as high and low pass filter signals. The peak amplitude is at 14 Hz. This is the dominant frequency of the original signal. Data measured with a frequency of approximately below 11 Hz is removed by a high-pass filter and data with a frequency of approximately above 8 Hz is removed by a low-pass filter.

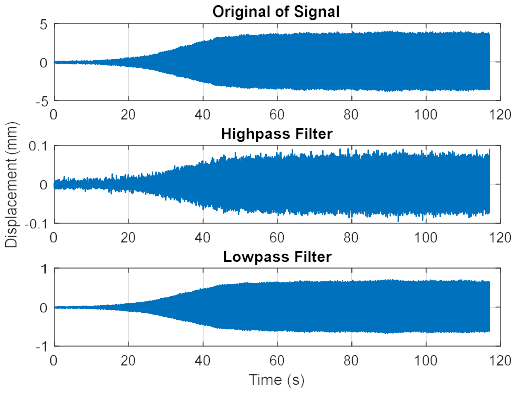

(a) Original signal, high-pass and low pass filter results

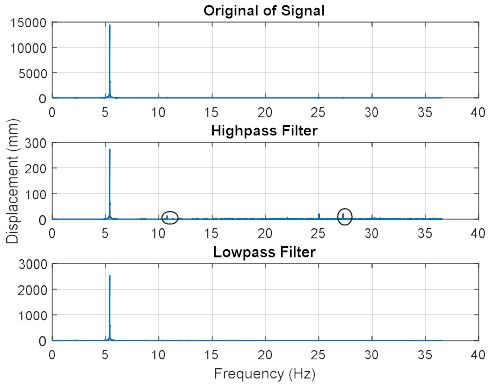

(b) Fast Fourier transform results of original signal, high-pass and low-pass filter

Figure 5. Fast Fourier Transform of signal measurement data using Daubechies wavelets

Figure 6 shows the simulation results of a circular cylinder vortex-induced response supported by an elastic cantilever beam with a Van der Pol oscillator model (Equation (28)).

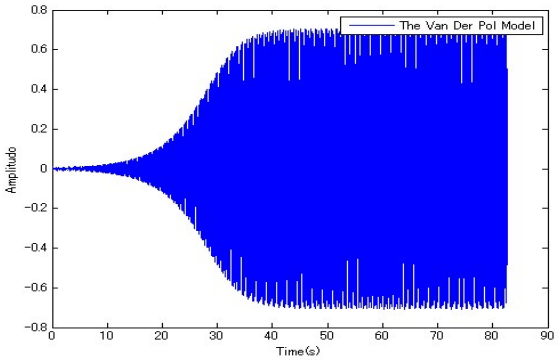

Figure 6. Simulation of vortex-induced cylinder model

Wavelet filter based on Daubechies wavelet and FxLMS algorithm with velocity learning μ = 0.008 applied to the time history of the Van der Pol wake oscillator model shown in Figure 7.

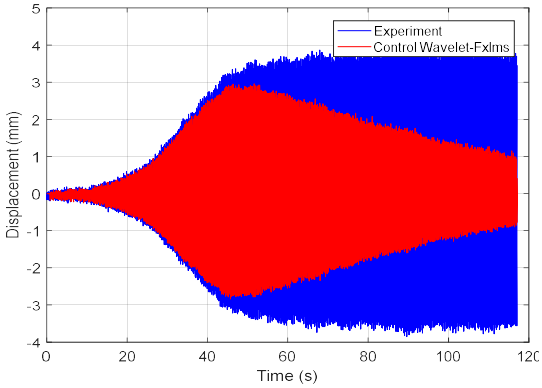

Figure 7. Comparison between time history of Van der Pol wake-up oscillator model and active control system with Daubechies wavele t filter -FxLMS, = 0.008

Adaptive filter with wavelet filter and FxLMS works as a vibration controller to reduce the amplitude. When the active nonlinear vibration controller is activated, with a time equal to 35 seconds, the amplitude decreases considerably after 55 seconds as shown in Figure 7. Note that the convergence time depends on the learning speed of the FxLMS algorithm; the greater the learning rate of the FxLMS algorithm, the faster the convergence.

Comparison of simulation results with wavelet filter and combination of wavelet filter and controller based on FxLMS (μ = 0.08) is shown in Figure 8 . The Van der Pol oscillator model consists of two sinusoidal components at 2 Hz and 3 Hz. The green line is the Van der Pol wake oscillator model. Figure 8(a) shows the frequency response of the Van der Pol oscillator model with a wavelet filter. The peak response amplitude with the wavelet filter at 3 Hz is 9 x 10^{-4} for Coiflets, 10 x 10^{-4} for Haar, 10 x 10^{-4} for Meyer, and 15 x 10^{-4} for Daubechies. Figure 8(b) shows the frequency response of the Van der Pol wake oscillator model with FxLMS. The peak amplitude of the wavelet filter response with FxLMS at 3 Hz is 6.1 x 10^{-4} for Coiflets, 6.61 x 10^{-4} for Haar, 6.81 x 10^{-4} for Meyer, and 7 x 10^{-4} for Daubechies.

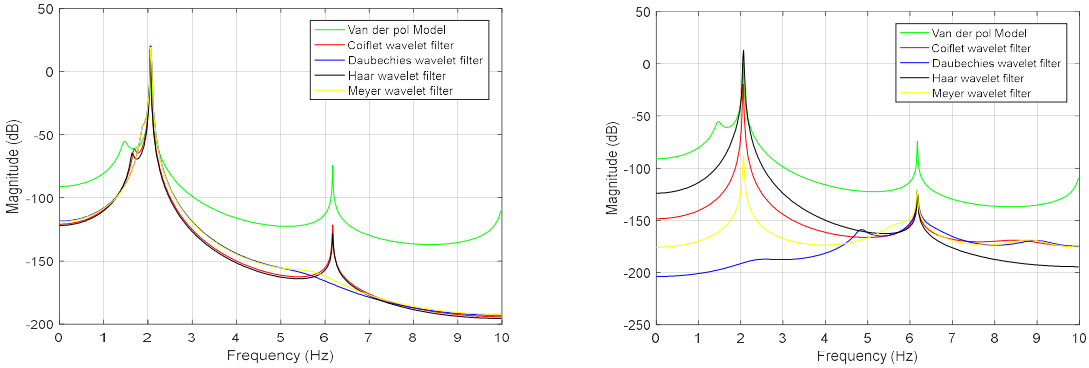

(a) Low pass filter **(b) High pass filter**

Figure 8. Cut-off frequency in wavelet type

However, for most practical filters, the high pass and low pass wavelet filter frequency levels above or below which the device fails to respond or operate efficiently are not the same. The difference between the frequency level above or below at which the device fails to respond or operate efficiently depends on the type of wavelet . The filter is described when the Coiflets wavelet with the FxLMS algorithm (μ = 0.008) with a magnitude of 44.3 dB is followed by a Meyer wavelet (μ = 0.008) with a magnitude of 43.6 dB. Meanwhile, the minimum global attenuation occurs when the Haar wavelet (μ = 0.0008) with a magnitude of 23.9 dB is followed by the Coiflets wavelet (μ = 0.0008) is 24.4 dB.

4. CONCLUSION

In this study, a description of the efforts to control the flow-induced vibration of an elastically supported structure in cross-flow. The effectiveness of the wavelet-FxLMS algorithm as an active nonlinear vibration control strategy has been successfully demonstrated both experimentally and theoretically under the Van der Pol wake oscillator.

CONFESSION

We would like to thank Prof. Dr. Yukinori Kebayashi from Hokkaido University who has facilitated us with the tools and equipment used in this research.

REFERENCES

Adewumi, G, & Inambao, F. (2017). Active Wind Turbine Aerodynamic Noise Control Using FXLMS Algorithm. *International Journal of Applied Engineering Research ISSN 0973-4562, 12*(24), 14382-14390.

Agung, W.B., & Anggraini, R., & Subekti, S. (2020). Development of Early Detection of Smoke and Gas Leaks in LPG Cylinders, Household Scale Fire Prevention (in Indonesia). *Exacta Factor, 13*(2), pp. 113-124.

Akansu, A.N., & Haddad, R.A. (2001). *Multiresolution Signal Decomposition: Transformations, Subbands and Wavelets*. New Work NM, Academic Press.

Akraminia, M., Mahjoob, M., & Tatari, M. (2017). Nonlinear Active Noise Control Using Adaptive Wavelet Filter. *American Scientific Research Journal for Engineering, Technology, and Sciences (ASRJETS), 37*(1), 287-304.

An, Fengyan, & Li, Hao. (2022). *Experimental Research on Reducing Flow-Induced Cavity Resonance with a Narrowband Active Noise Control System.* Citation: An, F.; Li, H.; Zhang, X.; Sun, C.; Liu, B. Experimental Research on Reducing Flow-Induced Cavity Resonance with a Narrowband Active Noise Control System. *Appl. Sci.*, *12*, 7044. https://www.mdpi.com/2076-3417/12/14/7044/pdf?version=1657861075

Babu, P., & Krishnan, A. (2010). A New Variable Threshold and Dynamic Step Size Based Active Noise Control System for Improving Performance. *International Journal of Computer Science and Information Security (IJCSIS), 7*(2), 160-165.

Bean, J.J., (2018). *Design and Analysis of an Active Noise Canceling Headrest*. https://vtechworks.lib.vt.edu/bitstream/handle/10919/94626/Bean_JJ_D_2018.pdf?sequence=1.

Blanchard, A., & Bergan, L.A. (2019*). Vortex-induced vibration of a linearly sprung cylinder with an internal rotational nonlinear energy sink in turbulent flow.* https://dspace.mit.edu/bitstream/handle/1721.1/131785/11071_2019_4775_ReferencePDF.pdf?sequence=1&isAllowed=y,.

Botti, N. (2021). *Active Structural-Acoustic Control on interior noise of a plate-cavity system using FxNLMS algorithm*. https://www.politesi.polimi.it/bitstream/10589/186212/4/2022_04_Botti_Botti.pdf.

Carra S., Amabili, M., Ohayon, R., and Hutin, PM. (2008). Active vibration control of thin rectangular plates in air or in contact with water in the presence of tonal primary disturbances. *Aerospace Science and Technology, 12,* 54–61.

Cao, S., He, Q., Zhang, R., & Cng, D. (2020). *Active Control Strategy of High-Speed Elevator Horizontal Vibration Based on LMI Optimization.* https://ceai.srait.ro/index.php?journal=ceai&page=article&op=download&path%5B%5D=6500&path%5B%5D=1564, 72-83.

Cong Le, D., Zhang, J., Li D., & Zhang, S. (2018). *A Generalized Exponential Functional Link Artificial Neural Networks Filter with Channel-Reduced Diagonal Structure for Nonlinear Active Noise Control*. https://www.sciencedirect.com/science/article/pii/S0003682X1731157X.

El-Shahed, R., Al berry, M., Ebied, H.M., & Shedeed, H.A. (2022). High capacity video hiding based on multi-resolution stationary wavelet transform and hybrid-matrix decomposition techniques. *Bulletin of Electrical Engineering and Informatics, 11(4),* pp. 1959~1969.

Fallah, M., & Imani, B.M. (2019). Adaptive inverse control of chatter vibrations in internal turning. *Mechanical Systems and Signal Processing 129*, 91-111.

Ishihara, T., & Li, T. (2019). *Numerical study on suppression of vortex-induced vibration of circular*. http://windeng.t.u-tokyo.ac.jp/ishihara/paper/2020-1.pdf,.

Kant, R., & Vinod, N. (2022). *A modified FxLMS uid flow control model for convectively*. https://www.ias.ac.in/article/fulltext/sadh/047/0104,.

Kobayashi, Y., Kamide, E., & Hoshino, Y. (2006). Clutch Cancellation and Vibration Cancellation Control of Elastic Supported Cylinders and Oscillator Build. *JSME Transactions (in Japanese).*

Kowalczyk, K., & Svaricek, F. (2005). Experimental Robustness FXLMS, and Distribution Algorithm for Active Control in Automotive Applications. *16th WOLD IFAC Congress: Prague*.

Krauze , P., & Kasprzyk, J. (2016). Mixture of Skyhook and FxLMS Control of a Half Car Model with Magnetorheological Damping. *Hindawi Publishing Corporation Advances in Acoustics and Vibration, Article ID 7428616, 13 pages*.

Lee, C.W. (2000). Uji Kinerja Sistem Active Engine Mount Pada Mobil Penumpang . *Kongres Internasional Ketujuh tentang Suara dan Getaran.* Jerman.

Liang, X., et al. (2022). *A New Proportionate Filtered-x RLS Algorithm for Active Noise Control System*. https://www.mdpi.com/1424-8220/22/12/4566/pdf?version=1655441503, *Sensors*, *22*, 4566.

Lu, L., & Yin, KL. et al. (2021). *A survey on active noise control techniques–Part I: Linear systems*. The work is supported by the National Science Foundation of P.R. China under Grant, Sichuan University Post doctoral Interdisciplinary Fund. https://arxiv.org/pdf/2110.00531.Malate, S.G. (1989). A Theory for Multiresolution Signal Decomposition: Wavelet Representation. *IEEE Trans. Anal Pattern. Mach. Intel., II(7).*

Luo, L., & Sun, Jinwei. (2018). *A novel bilinear functional link neural network filter for nonlinear active noise control*. http://www.elsevier.com/open-access/userlicense/1.0/,.

Morra P., et al. (2018). *Control OF Streaky Disturbances In The Boundary Layer Over A Flat Plate*. *31st congress of the international council of the aeronautical sciences.* Belo horizonte, brazil: http://www.icas.org/ICAS_ARCHIVE/ICAS2018/data/papers/ICAS2018_0473_paper.pdf.

Muslim, A.T., Subekti, S., Ali, I. K. (2022). Rancang Bangun Mesin Bubut CNC Berbasis Control MACH3. *SENASTIK Inovasi Teknologi dalam Menjawab Tantangan Revolusi Industri 4.0 di Era Pandemi*.

Nibourel, Pierre,. (2022). *Reactive control of 2nd Mack mode in a supersonic boundary layer with freestream velocity/density variations*. https://arxiv.org/pdf/2206.06224.

Niu, W., et al. (2019). Adaptive vibration suppression of time-varying structures with enhanced FxLMS algorithm. *Mechanical Systems and Signal Processing*, 93-107.

Olinto, C.R., Indrusiak, M.L.S, & Moler, S.V. (2006). Experimental Study of Bistable Flow in Tube Arrays, M. from Braz. soc. from *Mechanic. Science. & Eng. April- May, 2*(28), 233.

Padhi, T., Chandra, M., *et al.* (2018). New Hybrid Active Noise Control System with Combination of Convex Time and Frequency Domain Filtered-X LMS Algorithm. *Circuit System Signal Process, 37*, 3275–3294. https://doi.org/10.1007/s00034-018-0784-x.

Qiu, H., Lee, J., Lin, J., & Yu, G. (2006). Wavelet filter-based weak signature detection method and its application to rolling element bearing prognostication, *Journal of Sound and Vibration, 289*, 1066–1090.

Qiu, Z., Lee, C.M., Xu, Z.H., & Sui, L.N. (2016). Multi-resolution filtered-x LMS algorithm based on discrete wavelet transforms for active noise control. *Mechanical Systems and Signal Processing*, *66*, 458-469.

Shaharuddin, Nik M.R., & Darus, IZM,. (2013). *System Identification of Flexibly Mounted Cylindrical Pipe due to Vortex Induced Vibration*. https://www.academia.edu/download/31132208/1569694073.pdf.

Subekti1, S., Guntur, H.L., Djanali, V.S., & Syaifudin, A. (2022). *Simulation and Dynamic System Modeling in an Elastically Supported Rigid Cylinder for Vibration Energy Harvesting*. In:

Kolhe, M., Muhammad, A., El Kharbachi, A., Yuwono, T.Y. (eds) Recent Advances in Renewable Energy Systems. *Lecture Notes in Electrical Engineering*, *876*. Springer, Singapore. https://doi.org/10.1007/978-981-19-1581-9_7.

Subekti2, S., Setiawan, A.B., and Hammid, A. (2019). Simulation of Robot Arm for Diabetes Mellitus Patients. *Journal of Physics: Conference Series, 2nd International Conference on Advance & Scientific Innovation, Medan, Indonesia, 1424.*

Sun, Z., & Blu, T. (2022). A Nonlinear Steerable Complex Wavelet Decomposition Of Images. http://137,189.32.179/~tblu/monsite/pdfs/sun2201.pdf.

Tong, X., & Suh, C.S. (2014). Wavelet-Based LMS Filtered-X Algorithm for Permanent Magnet Synchronous Motor Control. *Proceedings of the 2014 ASME International Mechanical Engineering Congress and Exhibition*. *Volume 4B: Dynamics, Vibration, and Control*. Montreal, Quebec, Canada. (pp. 14–20). V04BT04A039. LIKE ME.

Wang, Enhao, & Xu, Wanhai . (2019). *The Effect Of Cubic Stiffness Nonlinearity On The Vortex-induced Vibration Of A Circular Cylinder At Low Reynolds Numbers.* https://strathprints.strath.ac.uk/76469/1/Wang_etal_OE_2019_The_effect_of_cubic_stiffness_nonlinear.

Wenchao, N., Chengzhe, Z., Bin, L., & Wei, W. (2019). Adaptive vibration suppression of time-varying structures with improved FxLMS algorithm. *Mechanical Systems and Signal Processing, 118*, 93–107.

Wu, Kevin, and Breuer, KS. (2006). *Control of the Turbulent Boundary Layer using FxLMS, Feed forward Architecture*. AIA.

Zhao, J., & Jacono, D. Lo. (2018). *Experimental investigation of in-line flow-induced vibration of a rotating circular cylinder*. https://oatao.univ-toulouse.fr/22882/1/Zhao_22882.pdf, https://doi.org/10.1017/jfm.2018.357.